

www.acsami.org Research Article

High-Sensitive Assay of Nucleic Acid Using Tetrahedral DNA Probes and DNA Concatamers with a Surface-Enhanced Raman Scattering/ Surface Plasmon Resonance Dual-Mode Biosensor Based on a Silver Nanorod-Covered Silver Nanohole Array

Chunyuan Song, Xinyu Jiang, Yanjun Yang, Jingjing Zhang, Steven Larson, Yiping Zhao, and Lianhui Wang*



Cite This: ACS Appl. Mater. Interfaces 2020, 12, 31242-31254



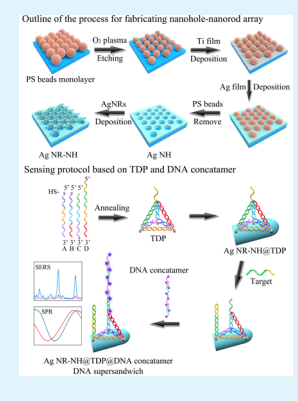
ACCESS

III Metrics & More

Article Recommendations

s) Supporting Information

ABSTRACT: A novel surface-enhanced Raman scattering/surface plasmon resonance (SERS/SPR) dual-mode biosensor prepared on a silver nanorod-covered silver nanohole (Ag NR-NH) array by surface modification of tetrahedral DNA probes is proposed for highly sensitive detecting nucleic acids by a special signal amplification strategy of DNA supersandwich. The Ag NR-NH with a large area and uniformly arrayed nanostructure possesses excellent anisotropic extraordinary optical transmission and strong localized surface plasmon resonance, which lead to sensitive SPR response to the change of a local refractive index and strong localized electric fields for excellent SERS activity. To obtain high sensitivity and specificity, smart tetrahedral DNA probes are immobilized onto the Ag NR-NH array and the DNA supersandwich sensing strategy, including the signal amplification of DNA concatamers, is used. About 10 times signal enhancement for SPR and 4 times for SERS are achieved by this sensing strategy. In the detection of the target DNA in the human serum, the two sensing modes have complementary performances, i.e., the limit of detection for the SPR array is high (0.51 pM), while for SERS, it is low (0.77 fM), but the specificity for SPR is much higher than that of SERS. This improves the robustness of the DNA sensors, and subsequent recovery tests also confirm good reliability of the



biosensor. The proposed SERS/SPR dual-mode biosensor has a great potential for high performance and reliable detection of trace disease-related nucleic acid biomarkers in the serum and is a powerful sensing platform for early-stage disease diagnosis.

KEYWORDS: SERS/SPR dual-mode biosensor, Ag NR-NH array, tetrahedral DNA probe, DNA concatamers, DNA supersandwich, nucleic acid

1. INTRODUCTION

Recently, plasmon-based chemical and biological sensors have been attracting extensive research attention due to the fact that they could offer a highly sensitive, label-free detection with low cost and a simple setup. 1-3 Most research and development efforts have been concentrated on how to design the optimal plasmonic nanostructures to achieve a higher sensitivity based on a single-plasmon detection principle⁴ or to improve the interaction between the surface of the plasmonic structures and targeted analyte molecules to achieve better specificity. However, with the improved sensitivity, the reliability of the sensor could be sacrificed. For example, a well-known plasmonic sensor, the surface-enhanced Raman scattering (SERS)-based optical sensor, has the advantages of ultrahigh sensitivity and spectral recognition of molecular fingerprint with envious specificity; sometimes, it could even achieve a single molecule detection. 5-12 Due to the exceptional sensitivity, SERS is very vulnerable to produce high background spectral signals from molecules adsorbed from the background (contaminations) or from other analytes presented in the detecting medium. This problem not only jeopardizes the true sensitivity for detecting

the targeted analyte due to high background signal and competitive adsorption of molecules to SERS "hot spots", increasing the chances to produce false-positive or false-negative signals, but also creates issues in practical application, such as shortening the shelfing time of the substrates or the need of a substrate cleaning method, which essentially increase the cost and make the detection procedure more complicated. A common strategy to improve the reliability of a high sensitivity sensor in the community is redundancy, ¹³ i.e., to use more than one sensor to detect the same targeted analyte. The redundant detection strategies not only could improve the robustness of the detection but also can improve the precision of the detection. However, the redundant detection strategy has seldom been

Received: May 8, 2020 Accepted: June 17, 2020 Published: June 17, 2020





used in plasmonic sensors. 14,15 Therefore, the combination of the two plasmonic sensing modes in one sensor (or sensing system) is expected to simultaneously coordinate their respective advantages and compensate each other's shortcomings to achieve an accurate and reliable detection. In fact, many different plasmonic sensing strategies share similar principles and are feasible to achieve such a redundant sensing strategy. For example, both the SERS- and localized surface plasmon resonance (LSPR)-based sensor all rely on the engineering of the local hot spots; thus, it is natural to combine SERS and LSPR together, as demonstrated by Potara et al. 16 Compared to LSPR, surface plasmon resonance (SPR) provides an even higher sensitivity and has already been commercially used for in situ, real-time, and label-free detecting or tracking the processes of biomolecular interactions at a metal interface. It would be great to combine SPR and SERS together to achieve a highly sensitive and robust sensing system. However, the sensing principles for SERS and SPR are very different: SERS relies on the generation of strong localized electric fields around a metallic nanostructure with a nonpropagating electromagnetic (EM) wave, while the SPR is based on the coupling of the incident EM wave to a propagating EM wave at the interface between a metal and a dielectric. Thus, it is very challenging to develop an SPR/ SERS dual-mode sensor.¹⁷ Nevertheless, the discovery of the extraordinary optical transmission (EOT) effect through nanohole arrays provides an alternative for SPR sensing. 18-Recently, Ai et al. used an elliptical Ag nanohole chip fabricated by nanosphere lithography to achieve a bulk index sensitivity of more than 700 nm/RIU based on EOT. ²² Carney et al. proposed a refractometric sensor with periodic nanoindented arrays created by holographic laser interference lithography and reached a sensitivity of 880 nm/RIU.²³ Meanwhile, the EOTactive nanohole arrays were also reported to have an SERS effect. 18,24 However, the SERS enhancement factor in these studies was not high due to the limited local electric field enhancement around the hot spots of the nanoholes. 18,25 So far, the SPR/SERS dual-mode biosensors based on nanoholes are rarely reported. Recently, our group reported a novel silver nanorod-covered silver nanohole array (Ag NR-NH). This structure exhibited an interesting dipole radiation-induced new EOT mode with strong local electric fields, 26 which is expected not only to possess good SPR sensing performance 22 but also to produce excellent SERS enhancement. In fact, our extensive previous studies indicate that tilted silver nanorod (Ag NR) arrays retain excellent SERS performance. 27-32 Therefore, we reasonably expect that the Ag NR-NH could have both SPR and SERS properties and is a good candidate for the development of high-performance SPR/SERS dual-mode sensors.

In addition to the use the SPR/SERS dual-mode sensor to guarantee the sensitivity and reliability, for developing excellent biosensors, the effective biological functionalization of the sensing surface with improved biological affinity and specificity is also crucial. Recently, three-dimensional DNA nanoprobes such as tetrahedral DNA probes (TDPs) have been reported to be immobilized on metal surfaces with programmable and controllable distribution and orientation so that high-affinity interfaces are achieved for specifically and efficiently capturing the target DNA molecules. Our previous work confirmed that the surface modification of TDPs could significantly enhance the response sensitivity of the interface to the change of the surrounding refractive index. Therefore, it is expected that a dual SPR/SERS biosensor modified by TDPs could have improved DNA detection performance.

Here, we have designed and fabricated a highly sensitive and robust SERS/SPR dual-mode nucleic acid sensor based on the TDP-modified Ag NR-NH array. To further improve the sensitivity, a special signal amplification strategy of DNA supersandwich by using DNA concatamers is also applied. The feasibility of the sensing mechanism has been confirmed by the polyacrylamide gel electrophoresis (PAGE) and step-bystep SPR monitoring, and the optimal sensing condition has been explored and obtained. About 10 times signal enhancement for SPR and 4 times for SERS have been achieved by the proposed DNA supersandwich sensing strategy. The two sensing modes have complementary performances, i.e., the SPR mode has a lower sensitivity but a higher specificity than that of the SERS. This improves the robustness of the DNA sensors, and subsequent recovery tests also confirm good reliability of the biosensor.

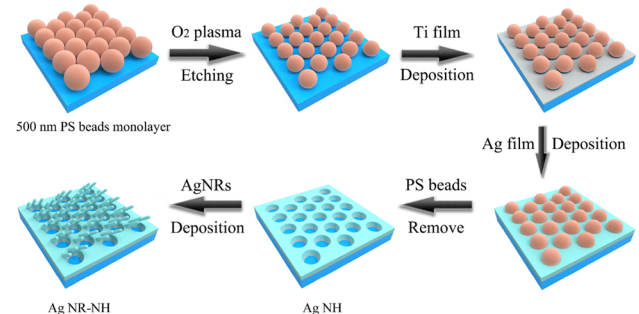
2. EXPERIMENTAL SECTIONS

2.1. Materials. Polystyrene beads with a diameter of 500 nm (Polyscience, USA) were used to form the colloid monolayer on glass slides (Gold Seal, USA) and silicon wafers (University Wafer, USA). Sulfuric acid (H2SO4; 98%, Fisher Scientific, USA), ammonium hydroxide (NH₄OH; 98%, Fisher Scientific, USA), and hydrogen peroxide (H2O2; 30%, Fisher Scientific, USA) were used to clean the glass and silicon substrates. The glass slides were cleaned by immerging in the boiling Piranha solution (H₂SO₄/H₂O₂ with a 4:1 ratio) for 30 min followed by water rinsing, and the silicon wafers were cleaned by a RCA-1 method (a solution of H₂O/H₂O₂/NH₄OH with a 5:1:1 ratio was heated to 70 °C) for 10 min followed by water rinsing (caution: the two washing solutions are very corrosive oxidizing agents, which should be handled with great care). Silver (99.99%, Plasmaterials, USA) and titanium pellets (99.995%, Kurt J. Lesker, USA) were used as the evaporation materials. 4-Mercaptophenol (Mph; 97%, Sigma-Aldrich, USA) was selected as the Raman test molecule. 1-Hexanol (C₆H₁₄O; 99%, Aladdin, China), chloroform (CHCl₃; 99%, Sinopharm Chemical Reagent, China), MeOH (CH₃OH; 99.5%, Sinopharm Chemical Reagent, China), acetone (CH3COCH3; 99.5%, Nanjing Chemical Reagent, China), and toluene (C7H8; 99.5%, Shanghai Lingfeng Chemical Reagent, China) were purchased to characterize the refractive index sensitivity (RIS) of the sensor. The single-stranded DNAs (ssDNAs) were synthesized and HPLC-purified by Sangon Biotech (Shanghai, China), and their names (abbreviations) and base sequences are listed in Table S1 (Supporting Information). Among them, three thiol-modified ssDNAs (i.e., A, B, and C) and a specially designed ssDNA D were used to assemble the TDP via the complementary hybridization of the same color-marked base sequences and leave the shadow-marked base sequence at the 5'-end of D free on a tip of the TDP. The target DNA (T) can be captured by the TDP via complementarily hybridize with D from the free shadow-marked base sequence to the green-marked sequence. As a result, the previously hybridized green-marked sequence at the 5'-end of C can be released, which can further capture the probe DNA. The probe DNAs are long double-stranded DNAs (dsDNAs), namely, DNA concatamers, and were prepared by the hybridization of DNA-S1 (S1) and DNA-S2 (S2) labeling ROX dye molecules at both their 3'- and 5'-ends. The capture DNA (C1) has a base sequence similar as the green-marked sequence of C. The single-base mismatched DNA (SM) with a single mismatched base marked in italic and unmatched DNA (UM) was designed as nonspecific test agents. Human serum (Biosharp, China) was used to prepare the analytes. Several different buffers, i.e., TM buffer (20 mM Tris, 50 mM MgCl₂, and pH 8.0), TBE buffer (89 mM Tris, 90 mM boric acid, 2 mM EDTA, and pH 8.0), TBE-Mg²⁺ buffer (89 mM Tris, 90 mM boric acid, 2 mM EDTA, and 12.5 mM MgCl₂), were prepared and used for the treatment of nucleic acids. Sterilized ultrapure Millipore water (18.2 M Ω ·cm) was used throughout all experiments. Unless otherwise specified, all chemicals and materials were used without further purification.

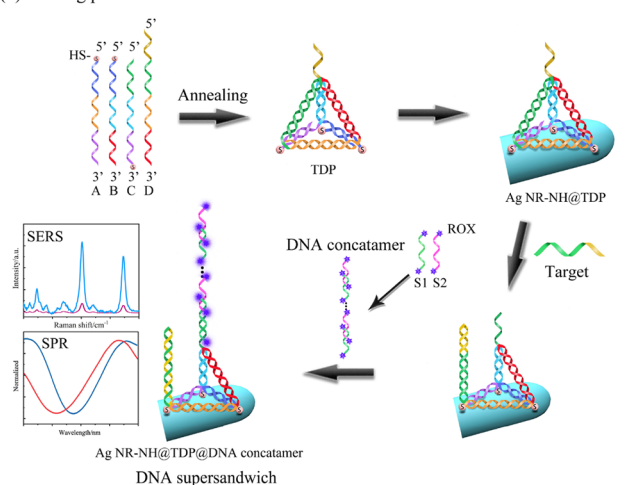
2.2. Fabrication of Ag NR-NH Arrays. The Ag NR-NH array was prepared by nanosphere lithography (NSL), reactive ion etching (RIE), physical evaporation deposition, and oblique angle deposition (OAD), as described in our previous work. ²⁶ The fabrication procedure is shown in Scheme 1a. First, 500 nm polystyrene beads were assembled as close-

Scheme 1. Schematic Illustrations of (a) the Fabrication of the Ag NR-NH Array and (b) the Proposed SERS/SPR Dual-Mode Sensing Strategy of DNA Supersandwich Using DNA Concatamers

(a) Outline of the process for fabricating nanohole-nanorod array



(b) Sensing protocol based on TDP and DNA concatamer



packed monolayers on clean glasses or silica wafers $(0.9 \times 2.5 \text{ cm})$ by the air-water interface method.³⁸ Then, the PS beads on the substrates were O₂ plasma-etched at a pressure of 40 mTorr with a 10 sccm oxygen flow, an inductively coupled plasma (ICP) power of 25 W, and a radio frequency power of 10 W for 350 s in a Trion Technology Phantom III RIE/ICP system to reduce their diameter. The etched substrates were positioned into a custom-designed electron beam deposition system with the substrate normal antiparallel to the incident vapor direction.^{27,39,40} A 10 nm layer of Ti was deposited at a rate of 0.2 nm/s followed by a 70 nm Ag film deposited at 0.3 nm/s under a high vacuum condition ($<3 \times 10^{-6}$ Torr). The film thickness and deposition rate were monitored by a quartz crystal microbalance (QCM). The PS beads on the substrates were then removed by Scotch tapes followed by rinsing with toluene to remove residual PS beads. After several water rinses, the Ag nanohole (NH) arrays were obtained. Then, the substrates were reloaded into the deposition chamber and an oblique angle deposition (OAD) was performed to deposit Ag NR on the NH array: the substrate normal was rotated to 86° with respect to the incident vapor direction, a 250 nm layer (QCM reading) of Ag NR was deposited at a rate of 0.3 nm/s, and then, the Ag NR-NH arrays were obtained. As a control, the Ag NR arrays without NHs were deposited directly on the flat glasses or silica substrates under the same OAD conditions. The anisotropic transmission properties of the Ag NR-NH and Ag NR arrays were characterized by linearly polarized lights from 0° to 90° with respect to the long axis of the Ag NRs at an interval of 10°.

The SERS characterization was performed by immerging the resulting substrates in 1 M Mph overnight followed by SERS measurements with a 633 nm excitation laser, 1% laser power, $20\times$ objective lens, and 1 s acquisition time.

- **2.3. Preparation of TDPs.** The TDPs were assembled by the hybridization of A, B, C, and D ssDNAs, as shown in step 1 in Scheme 1b. Briefly, equimolar quantities of four ssDNAs were mixed in 300 μ L of a TM buffer and annealed for 5 min at 95 °C to assemble the TDPs with a final concentration of 1 μ M. To characterize the formation of TDP, 10% native polyacrylamide gel electrophoresis (PAGE) was performed in 1× TBE-Mg²⁺ buffer (ice bath) with a voltage of 80 V for 120 min.
- **2.4. Modification of TDPs on Ag NR-NH Arrays.** The TDPs were immobilized on the Ag NR-NH arrays by the three sulfhydryl groups on the bottom of the TDPs via the formation of Ag—S covalent bonds (step 2 in Scheme 1b). Briefly, 300 μ L of 1 μ M TDP was diluted into 3 mL by a TM buffer, and then, the Ag NR-NH arrays were immersed into the TDP solution overnight at 25 °C. After TM buffer rinsing, the TDP-modified Ag NR-NH arrays (Ag NR-NH@TDP, i.e., SPR/SERS dual-mode biosensor) were obtained and stored in a TM buffer at 4 °C. The surface modifications were monitored by measuring the anisotropic transmission spectra of the Ag NR-NH array under the unpolarized, 0°, and 90° linear polarized lights. This substrate could be used to directly detect the targeted DNAs (step 3 in Scheme 1b).
- **2.5. Preparation of DNA Concatamers.** DNA concatamers were assembled by the hybridization chain reaction between DNA S1 and DNA S2 (the inset step 4 in Scheme 1b). Briefly, 160 μ L of a TM buffer containing 3.75 μ M S1 and 3.75 μ M S2 was annealed by heating at 95 °C for 5 min and then cooled down to room temperature gradually. Then, the solution was incubated at 25 °C for 3 h to form the DNA concatamers via the hybridization of complementary sequences of S1 and S2 marked in the same color (Table S1). The DNA concatamers were then diluted into 3 mL by a TM buffer and restored at 4 °C for further usage. To verify the assembly of DNA concatamers, a 10% native PAGE gel was run in 1× TBE-Mg²⁺ buffer with a stable voltage of 80 V for 120 min.
- 2.6. SERS/SPR Dual-Mode Sensing Protocol. The SERS/SPR dual-mode sensing strategy was verified on the Ag NR-NH@TDP via the formation of DNA supersandwich structures, as shown in Scheme 1b. Specially, once the target DNA is incubated with the Ag NR-NH@ TDP biosensor, the TDPs can capture the target DNAs and release the previously hybridized green-marked sequence at the 5'-end of C. The released sequence can further capture the DNA concatamer to form a Ag NR-NH@TDP@DNA concatamer supersandwich structure (step 4 in Scheme 1b). Due to the target DNA-mediated linkage of DNA concatamers on the Ag NR-NH@TDP, a significant RI response may occur. In addition, the ROX dye molecules from DNA concatamers can produce significantly an SERS signal under the laser irradiation. In contrast with the classical TDP for the sandwich sensing strategy with a base sequence (capturer) at the tip of the tetrahedron, the proposed TDP can undergo deformation under the trigger of the target and then open the tetrahedral structure, resulting in releasing the previously hybridized green-marked sequence at the 5'-end of C as the capturer for further capturing the DNA concatamers. The proposed TDPs can provide the capturer with more bases for the hybridization with the DNA concatamers compared to the classical TDPs, which can significantly improve the capture efficiency of the DNA concatamers and obtain more sensitive detection. The sensing protocol was carried out as follows. Briefly, the Ag NR-NH@TDP arrays were immerged into 3 mL of target DNA with different concentrations diluted in a TM buffer or 10% human serum and incubated for 3 h at 25 °C. After thorough washing, each biosensor was incubated with 3 mL of DNA concatamer solution for 3 h at 25 °C to capture DNA concatamers by the specific hybridization between the complementary bases of TDPs and DNA concatamers followed by TM buffer washing. The transmission spectra of the biosensors were measured after each step under the unpolarized, 0°, and 90° linear polarized lights. The SERS spectra were collected immediately on the wet biosensors, which were rinsed by a TM buffer.

2.7. Instruments. Scanning electron microscopy (SEM) images were obtained by a FEI Inspect F SEM (FEI, USA). An Imagel software (NIH, USA) was used to analyze the SEM images. The polyacrylamide gel electrophoresis (PAGE) was run by a 165-8001 mini-PROTEAN Tetra vertical electrophoresis system (BIO-RAD, USA) and imaged by a GeneSys system (Syngene, UK). The transmission spectra were collected by a UV-3600 UV-vis-NIR spectrophotometer (Shimadzu, Japan) from 300 to 1800 nm. The polarized angle-dependent transmission spectra were performed by positioning two polarizers into the sample and reference light paths of the UV-vis-NIR spectrophotometer via a homebuilt bracket. A polarization angle of 0° was defined as the angle between the E-field of the incident light and the long axis direction of the NRs. Unless otherwise stated, the transmission measurements were performed by immerging the arrays into a TM buffer in a quartz cuvette. The SERS measurements were performed by a Renishaw InVia confocal Raman microscope (Renishaw, UK), and unless otherwise specified, the measurement parameters were set to be an excitation wavelength of 633 nm, 1% laser power, 20× objective lens, and 1 s acquisition time. For each characterization, 15 SERS scans were collected at different positions on the Ag NR-NH to obtain an averaged SERS spectrum and the baselines were subtracted by a software Wire 4.3 (Renishaw, UK).

3. RESULTS AND DISCUSSION

3.1. Characterizations of Ag NR-NH Arrays. 3.1.1. Morphology. Figure 1 shows the representative top and crosssection view SEM images of the Ag NH and Ag NR-NH arrays. The Ag NH array shown in Figure 1a reveals high-quality, largearea, uniform, and hexagonal latticed nanoholes. According to the magnified top and cross-section view SEM images shown in the inset and bottom, respectively, the diameter of nanohole is D= 339 \pm 9 nm, the lattice spacing is L = 500 \pm 10 nm, and the height of the Ag film is $h = 85 \pm 2$ nm. For the Ag NR-NH array (Figure 1b), randomly distributed tilted Ag NRs are only grown on the ridges of the nanoholes or Ag thin film area, with the NR length $l = 151 \pm 40$ nm, the NR density $\eta = 53 \pm 6$ NR/ μ m², and the tilting angle (defined in Figure 1b) $\beta = 69^{\circ} \pm 4^{\circ}$. Note that no NRs were grown inside the nanoholes. The X-ray diffraction (XRD) pattern of the Ag NR-NH array (Figure S1) shows the peak corresponding to the (111) plane of Ag.

3.1.2. Optical Properties. Figure S2a,b shows the polarization-dependent transmission spectra $T(\lambda, \varphi)$ of the Ag NH and Ag NR-NH arrays measured at the polarization angle φ from 0° to 90° with an interval of 10° . The $T(\lambda, \varphi)$ for the Ag NH array is clearly independent on φ , while it varies significantly with φ for the Ag NR-NH array. Figure 2a-c compares the $T(\lambda,0^{\circ})$ and $T(\lambda,90^{\circ})$ spectra of the Ag NH, Ag NR, and Ag NR-NH arrays. Both the $T(\lambda,0^{\circ})$ and $T(\lambda,90^{\circ})$ spectra of the Ag NH array (Figure 2a) show four characteristic peaks/valleys marked as V_1 , P_1 , V_2 , and P_2 , respectively. Both P_1 ($\lambda_{P_1} \sim 540$ nm) and P_2 $(\lambda_{P_2} \sim 840 \text{ nm})$ are assigned to the (1,0) EOT resonance peaks at the Ag/glass and Ag/air interfaces, respectively, whereas V_1 $(\lambda_{V_1}\sim 430 \text{ nm})$ and V_2 $(\lambda_{V_2}\sim 660 \text{ nm})$ are the (1, 0) Ag/glass and Ag/air transmission minima, respectively, due to Wood's anomaly.²⁶ For the Ag NR array, as shown in Figure 2b, the $T(\lambda,0^{\circ})$ spectrum shows a broad, low transmittance at λ >500 nm, while the $T(\lambda,90^{\circ})$ exists a dip at $\lambda \sim 400$ nm. This φ dependent $T(\lambda)$ is consistent with previous reports.⁴¹ The $T(\lambda)$ φ) of the Ag NR-NH array (Figure 2c) shows rich spectral features and also strong φ dependence. The $T(\lambda,90^{\circ})$ resembles the spectra of the Ag NH arrays with four peaks/valleys appearing at almost the same wavelength positions, while the $T(\lambda,0^{\circ})$ shows a new EOT peak P_3 located at $\lambda_{P3} \sim 1360$ nm, as reported in ref 26. Figure 2d shows the SERS spectra of Mph

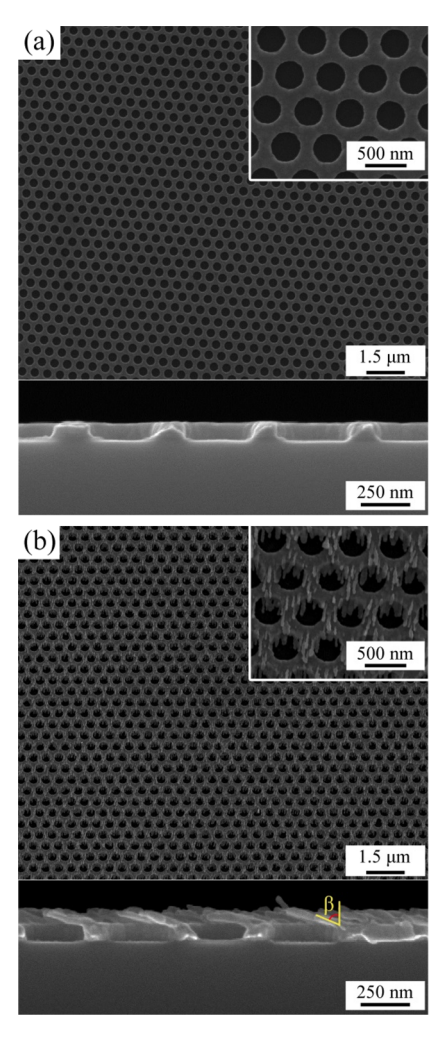


Figure 1. SEM characterization of Ag NH and Ag NR-NH arrays. (a) Top view SEM image of the Ag NH array (inset: magnified image) and the cross-section view SEM (bottom). (b) Top view SEM image of the Ag NR-NH array (inset: magnified image) and the cross-section view SEM image (bottom).

obtained from Ag NH, Ag NR, and Ag NR-NH arrays, and the characteristic SERS peaks are ascribed to different molecular vibrational modes of Mph. The results indicate that the Ag NR-NH array produces a better SERS signal compared to that of the Ag NR array directly deposited on the Si wafer (without nanoholes). In fact, the SERS enhancement factor (EF) of the Ag NR-NH was determined to be 4.02 \times 10, and the corresponding SERS and normal Raman spectra (Figure S3) as well as the detailed calculation can be found in Section S4. Furthermore, a theoretical study on the special EOT effect and good SERS activity of the Ag NR-NH array by finite-difference time-domain (FDTD) calculations can be found in our previous paper.

3.1.3. RIS of the Ag NR-NH Array. The RIS of the Ag NR-NH array was characterized by immersing the Ag NR-NH array in MeOH (n = 1.328), acetone (n = 1.359), 1-hexanol (n = 1.418), chloroform (n = 1.446), and toluene (n = 1.496) followed by measuring the unpolarized $T(\lambda)$, $T(\lambda,0^{\circ})$, and $T(\lambda,90^{\circ})$. Figure 3a,c,e shows the RI-dependent $T(\lambda)$, $T(\lambda,0^{\circ})$, and $T(\lambda,90^{\circ})$, respectively. The peak/valley positions as indicated in the spectra exhibit significant polarization dependence. Figure 3b,d,f plots the corresponding peak and valley wavelengths versus RI, and the corresponding RIS is extracted from linear fitting.

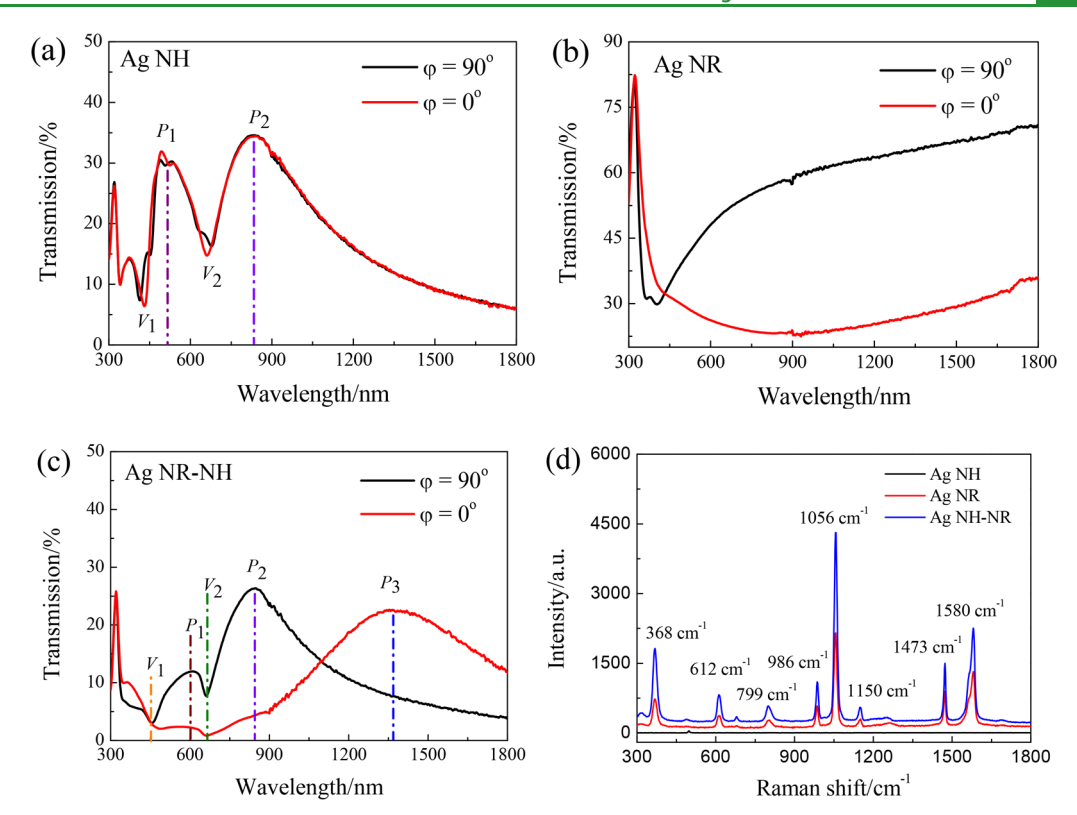


Figure 2. Transmission spectra of (a) Ag NH, (b) Ag NR, and (c) Ag NR-NH recorded at the polarization angle $\varphi = 0^{\circ}$ and 90° , respectively. (d) SERS spectra of Mph obtained from Ag NH, Ag NR, and Ag NR-NH arrays.

Regardless of the polarization, the V_2 peak gives an RIS of ~400 nm/RIU and present a sharp dip in $T(\lambda)$ and $T(\lambda, \varphi)$; therefore, the V_2 peak is chosen as the characteristic feature for further index sensing.

3.2. Characterization of the DNA Targeting Mechanism. 3.2.1. PAGE Characterization. Figure 4 shows the PAGE characterization of the DNA probe formation and targeting for the SERS/SPR dual-mode sensing. The schematic diagram of TDP formation and subsequent hybridization with target DNA is illustrated in Figure 4a (left), and the resulting electrophorogram is shown in the right panel. The nine lanes represent various DNAs and DNA assemblies, including the single DNA solutions of A, B, C, D, and T (lanes 1 and 6-9) and assemblies of A + B, A + B + C, A + B + C + D (i.e., TDP), and TDP + T(lanes 2-5), respectively. According to lanes 1-3 and a single narrow, clear band shown in lane 4, it is clear that the TDPs were self-assembled with a high yield. The slightly different location of the band in lane 5 (TDP + T) compared to that of lane 4 indicates the efficient hybridization of TDP with the target DNA (T). Figure 4b shows the schematic diagram and electrophorogram of the formation of DNA concatamers and DNA supersandwich, characterizing by the PAGE of C1, S1, S2, S1 + S2 (i.e., DNA concatamer), S1 + S2 + C1, S1 + C1, and S2 + C1. The top stripe in lane 4(S1 + S2) indicates the formation of the DNA concatamer, while a small amount of free S1 and S2 (bottom faint stripe) was left in the mixture. Lane 5 illustrates the result of the hybridization of the DNA concatamer with C1. The slow-moving top stripe is ascribed to the hybrid of C1 and DNA concatamer, the bottom stripe belongs to the different free S1, S2, or C1, and the two middle stripes could correspond to the DNA structures partially hybridized between S1, S2, and C1. The stripe in lane 6 shows the efficient hybridization of S1 and C1, while the two stripes in lane 7 (a very faint stripe is close to

the bottom) represent the separated S2 and C1 mixture if compared to the results from lanes 1 and 3. These results demonstrate the successful formation of TDPs and DNA concatamers and the specific and efficient hybridizations of target DNA with TDP as well as TDP with DNA concatamers, respectively.

3.2.2. SPR Characterization of the Surface Modification of the Ag NR-NH Array. Figure 5 shows the SPR characterization of the step-by-step surface modifications of the Ag NR-NH array by measuring $T(\lambda)$ (Figure 5a), $T(\lambda, 0^{\circ})$ (Figure 5c), and $T(\lambda, 0^{\circ})$ 90°) (Figure 5e) where Figure 5b,d,f shows the corresponding enlarged normalized spectra at V_2 , respectively. The shift of the $\operatorname{dip} V_2$ after each immobilization step is shown in Figure S4. With the increased steps of surface immobilization, i.e., modified TDP, T, and DNA concatamer in sequence, the dip V_2 redshifts more and more. In particular, the SPR shifts of the dip V_2 after the combination of target are 1 nm unpolarized, 1.5 nm 0° polarized, and 0.5 nm 90° polarized conditions. By introducing the DNA concatamer in the sensing strategy, the shifts of the dip V_2 amplified to 8.5, 8.2, and 8 nm unpolarized, 0° polarized, and 90° polarized conditions, respectively, which means that the SPR sensitivity can be improved about eight times by using the DNA concatamer relative to the direct detection of target without the signal amplification of DNA concatamers. The significantly amplified SPR shift is mainly attributed to the large structure of DNA concatamers, which can cause more significant changes in the interfacial refractive index than the small structure target molecules. These results demonstrate that RIS of the molecular index sensing of the Ag NR-NH array is very significant to the formation DNA super structures on the surface.

3.3. SERS/SPR Dual-Mode Sensing Characterizations. 3.3.1. SERS/SPR Dual-Mode Sensing Target DNA in Buffer. Figure 6 shows the $T(\lambda)$ (Figure 6a), $T(\lambda, 0^{\circ})$ (Figure 6c), and

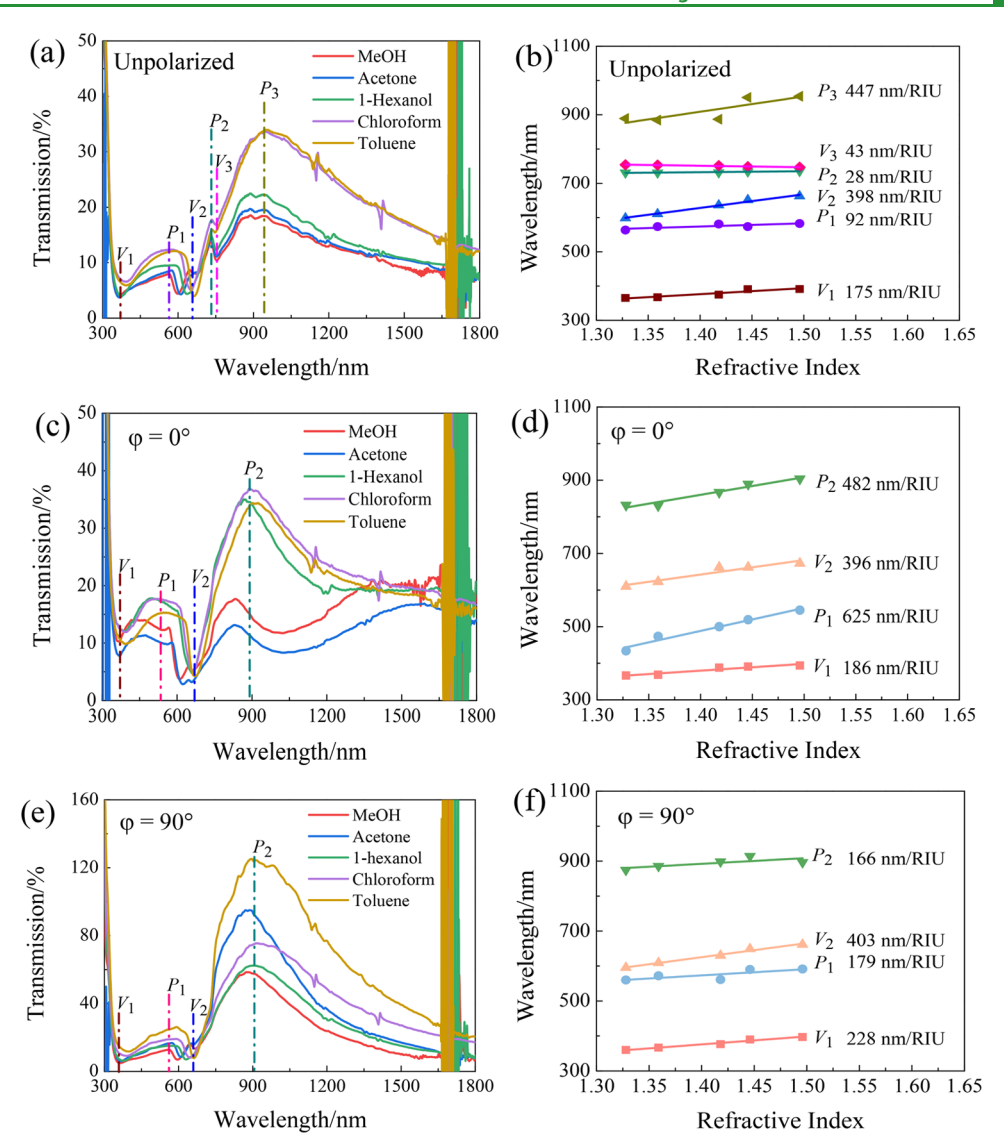


Figure 3. RI sensing performance characterization of the Ag NR-NH array: the RI-dependent transmission spectra under the (a) unpolarized, (c) 0° polarized, and (e) 90° polarized lights and the (b, d, f) corresponding plots of the RI-dependent wavelength of the peaks and valleys obtained from corresponding spectra.

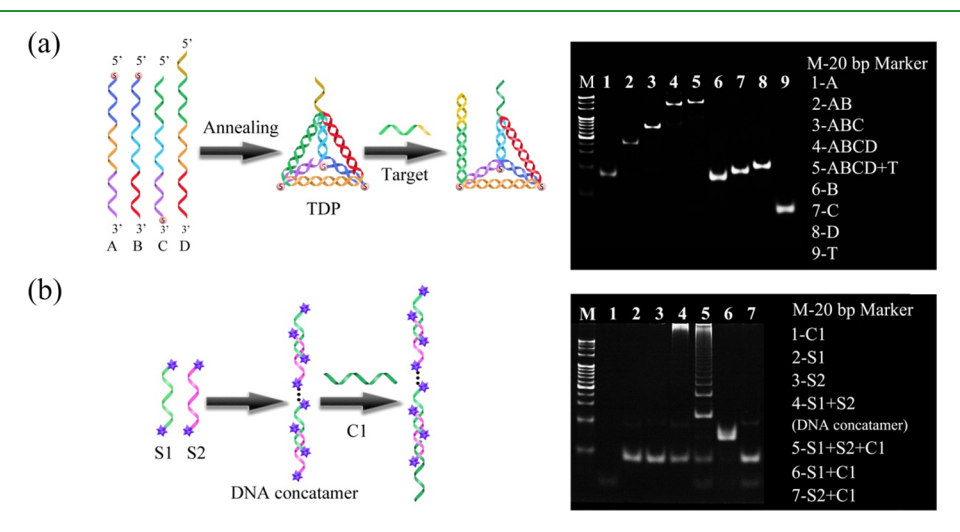


Figure 4. PAGE characterization of the TDP and sandwich DNA structures. (a) Schematic diagram and PAGE analysis of the formation of TDP. (b) Schematic diagram and PAGE analysis of the formation of DNA concatamers and their hybridization to C1.

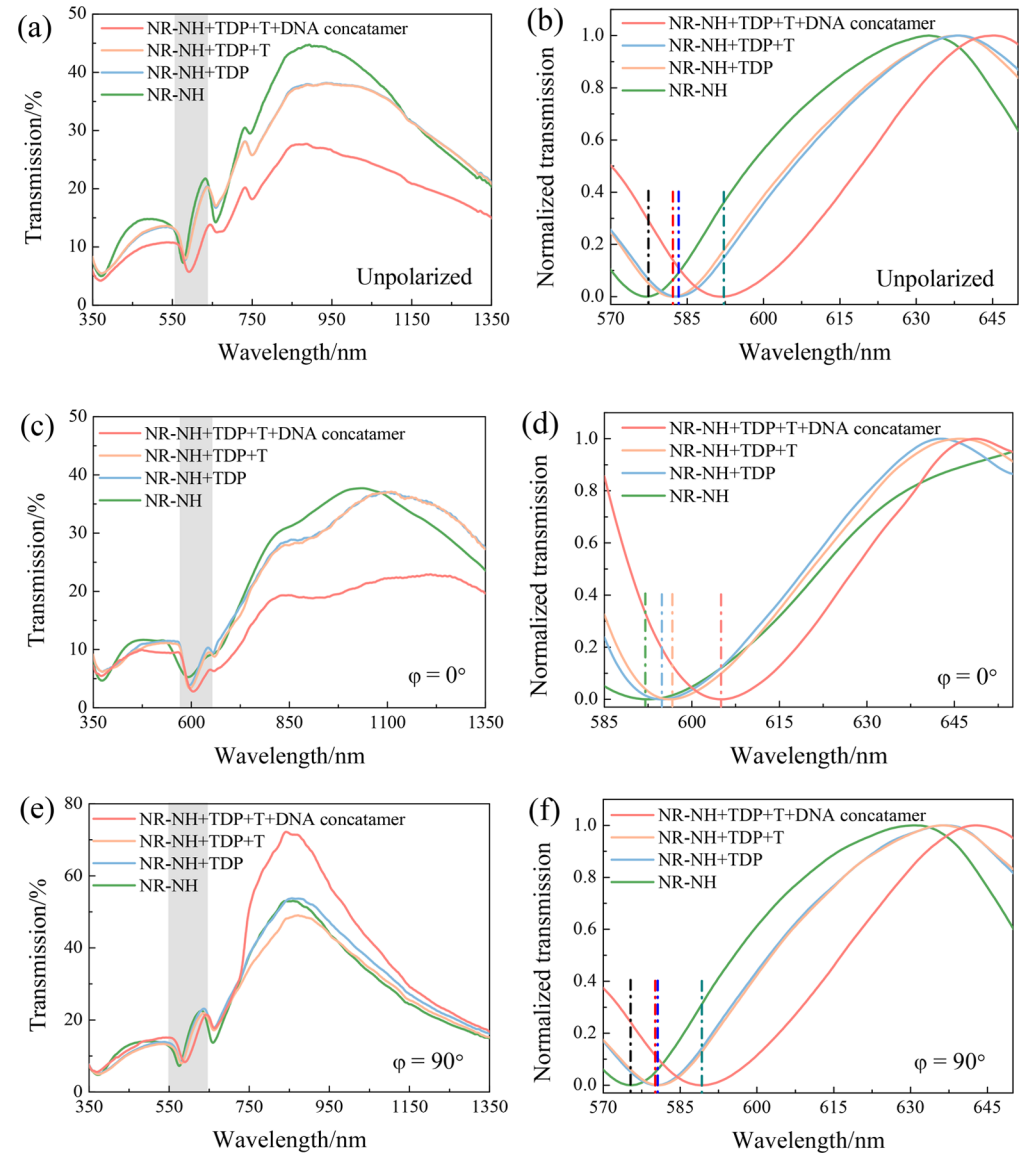


Figure 5. SPR characterizations of the surface modifications of the Ag NR-NH array: the transmission spectra under the (a) unpolarized, (c) 0° polarized, and (e) 90° polarized lights and the (b, d, f) corresponding enlarged spectra around V_2 .

 $T(\lambda, 90^{\circ})$ (Figure 6e) of the TDP-modified Ag NR-NH array after immersed in different concentrations of T in a TM buffer $(C_T = 1 \text{ pM}, 5 \text{ pM}, 10 \text{ pM}, 50 \text{ pM}, 100 \text{ pM}, 500 \text{ pM}, 1 \text{ nM}, 5 \text{ nM},$ and 10 nM, respectively) and a blank control (i.e., TM buffer without T). The corresponding shifts of the V_2 dip $(\Delta \lambda)$ versus $\log C_{\rm T}$ (semi-log scale) are plotted in Figure 6b,d,f. All $\Delta \lambda - \log$ $C_{\rm T}$ follow a linear relationship with $\Delta \lambda = 1.96 \times \log C_{\rm T} + 25.2$ (R^2 = 0.968) for $T(\lambda)$, $\Delta \lambda = 1.96 \times \log C_T + 26.3$ ($R^2 = 0.994$) for $T(\lambda,90^{\circ})$, and a bad linear relationship $\Delta\lambda = 2.75 \times \log C_{\rm T} + 36.7$ $(R^2 = 0.713)$ for $T(\lambda,0^\circ)$. The fitting slopes for $T(\lambda)$ and $T(\lambda,90^{\circ})$ are the same, indicating that the effective RIS for both configurations is the same. By defining the limit of detection (LOD) as the lowest concentration that produces a signal 3 times stronger than the standard deviation of the blank control, 31,32,42 the LODs of the TDP-modified Ag NR-NH array were calculated to be 0.27 pM for $T(\lambda)$ and 0.18 pM for $T(\lambda,90^{\circ})$. Both are in a similar order of magnitude, but for $T(\lambda,90^{\circ})$, it seems to give a better LOD.

The SERS spectra for the same samples immersed in T with different concentrations $C_{\rm T}$ are shown in Figure 7a. Each

spectrum in Figure 7a was averaged from 15 measurements, and the spectral uniformity is demonstrated in Figure S5, showing a <5% variation in peak intensity. Two dominant peaks at $\Delta \nu$ = 1500 and 1650 cm⁻¹ are visible, and their peak intensities increase monotonically with $C_{\rm T}$. Figure 7b plots the SERS peak intensity I_{1500} at $\Delta \nu$ = 1500 cm⁻¹ versus log $C_{\rm T}$, and a good linear relationship can be obtained with I_{1500} = 860 × log $C_{\rm T}$ + 13,800 (R^2 = 0.990) and an LOD of 0.38 fM. The LOD obtained from SERS is about 3 orders of magnitude lower than that of the index sensing configuration. Also, the SERS measurements provide a wider linear detection range (or dynamics range, from 1 fM to 10 nM) compared to that (from 1 pM to 10 nM) of the index sensing. All these make the SERS/SPR dual-mode sensor more sensitive and have a better performance.

3.3.2. Specificity of the SERS/SPR Dual-Mode Sensing. The specificity characterization of the proposed SERS/SPR dual-mode assay is shown in Figure 8 by testing the specific DNA T (100 pM), unspecific SM, and UM (1 nM). The $T(\lambda,90^\circ)$ after targeting T, UM, and SM is shown in Figure 8a,b, respectively. The V_2 dip redshifts significantly after the TDP-modified Ag

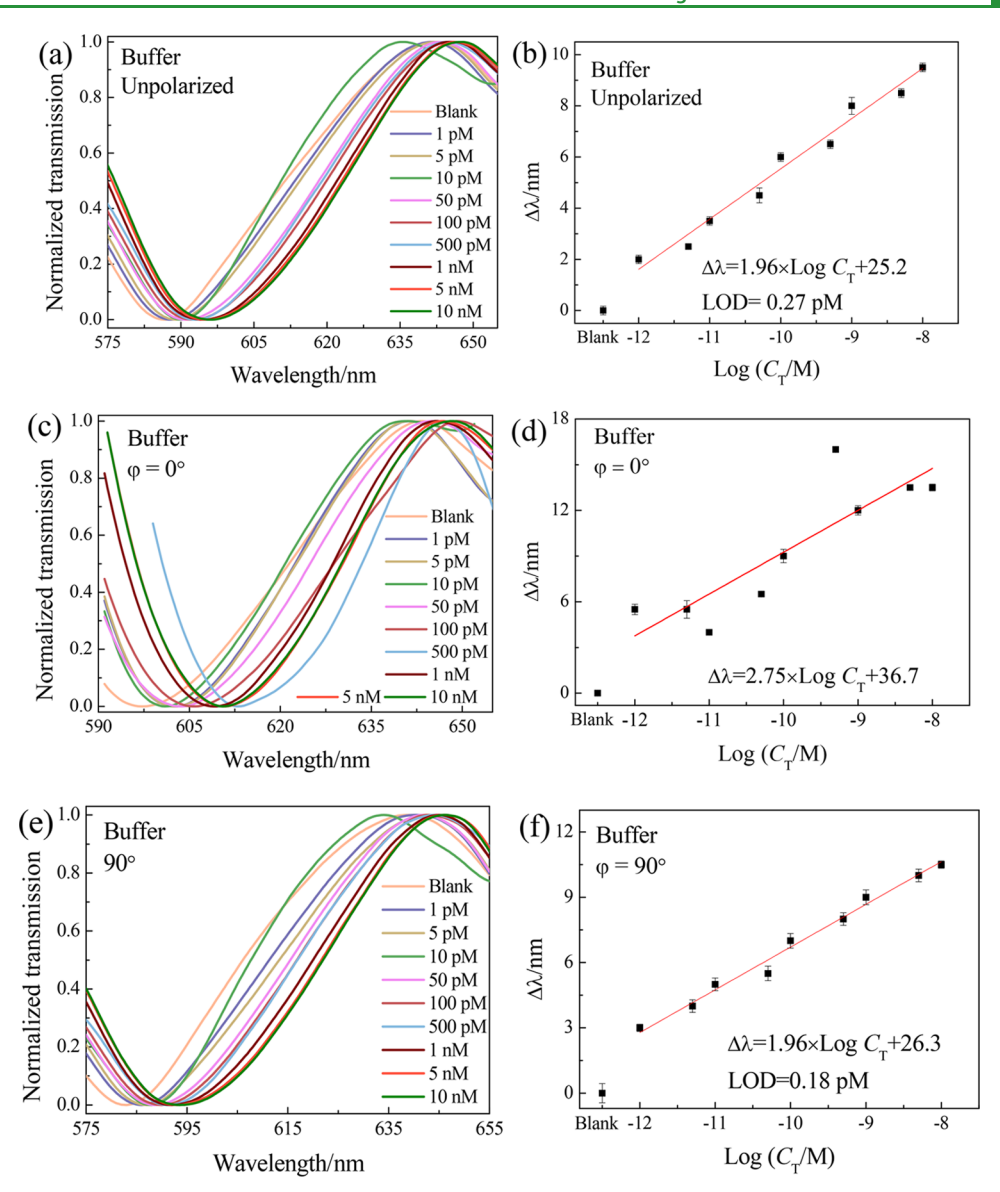


Figure 6. SPR assay for targeted DNA T in a TM buffer: the concentration-dependent normalized transmission spectra under the (a) unpolarized, (c) 0° polarized, and (e) 90° polarized lights and the (b, d, f) corresponding semi-log plots of $\Delta\lambda$ of the dip V_2 versus C_T . Statistics were obtained by three measurements (n = 3).

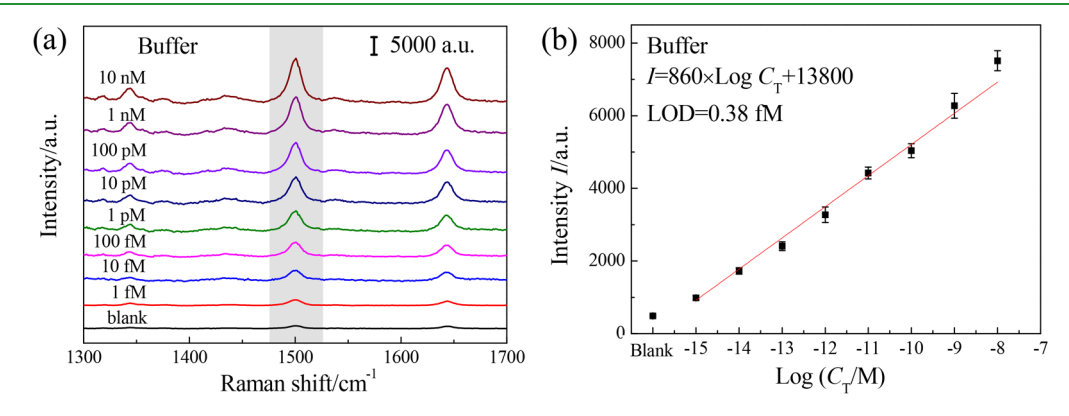


Figure 7. SERS assay for the target DNA T in a TM buffer. (a) Concentration-dependent SERS spectra. (b) Semi-log plot of the SERS peak intensity I_{1500} versus C_T . Statistics were obtained from 15 measurements (n = 15).

NR-NH array immersed to only 100 pM T (Figure 8a), while there is almost no shift observed after immersing in 1 nM SM and UM (Figure 8b). The SERS spectra in Figure 8c show

similar but slightly different results. Both the SERS spectra after targeting T and SM show significant changes in peak intensities, while the spectrum is insensitive to UM. Note that the

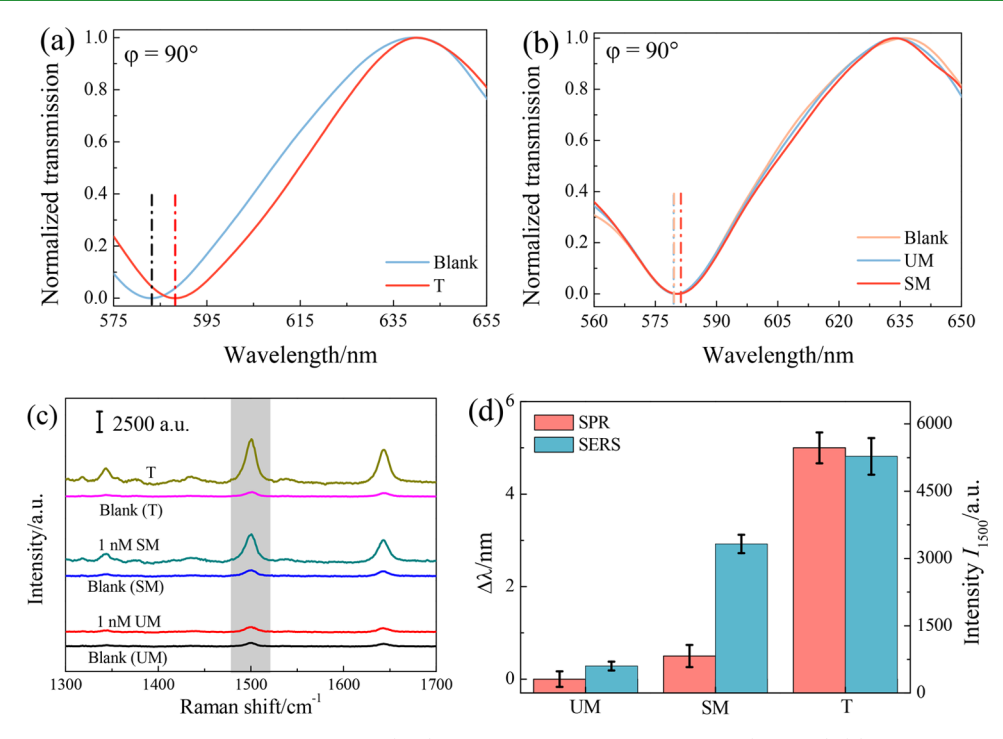


Figure 8. Specificity of the SERS/SPR dual-mode biosensor. (a, b) Normalized transmission spectra ($\varphi = 90^{\circ}$) (a) before and after immersing in 100 pM DNA T solution and (b) before and after immersing in unspecific 1 nM UM and SM solutions. (c) SERS spectra before and after immersing in T, UM, and SM solutions. (d) Summary of the transmission peak shift $\Delta\lambda$ and SERS peak intensity I_{1500} after immersing in T, UM, and SM solutions.

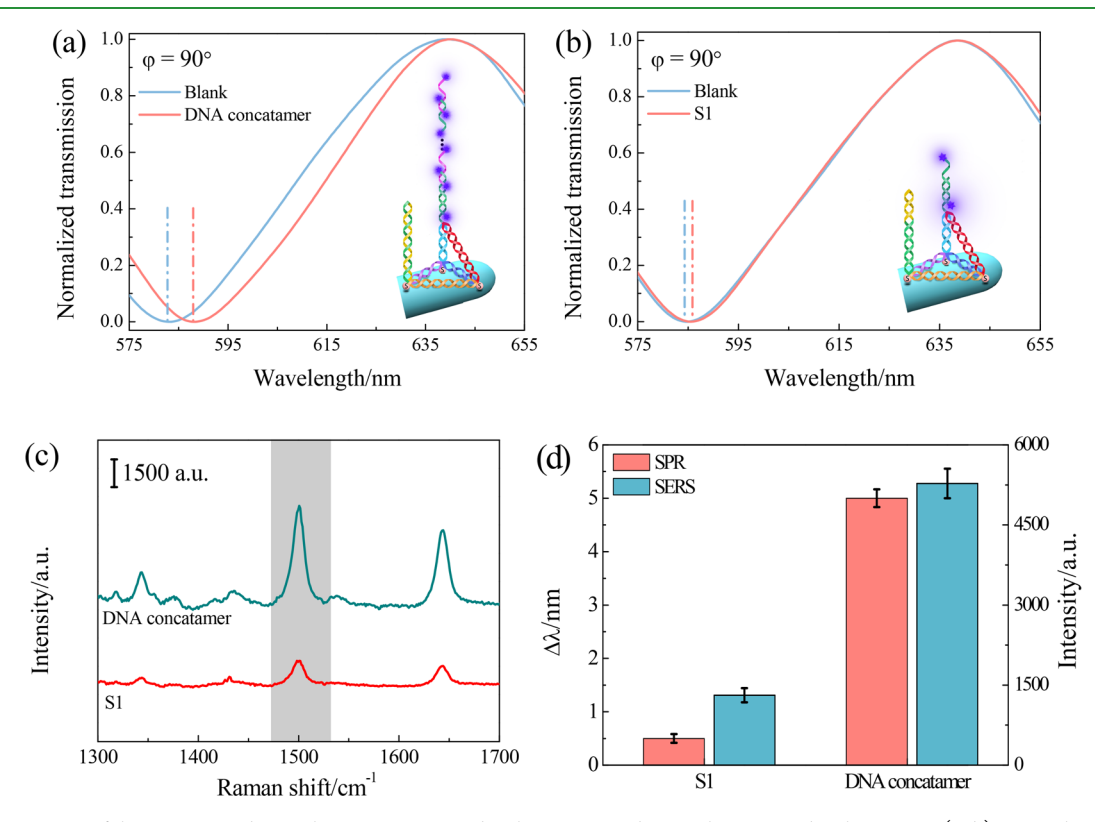


Figure 9. Comparison of the sensitivity due to the DNA supersandwich strategy and normal DNA sandwich strategy. (a, b) Normalized transmission spectra ($\varphi = 90^{\circ}$) (a) before and after DNA concatamer strategy and (b) before and after the normal ssDNA S1 DNA sandwich strategy. (c) Corresponding SERS spectra. (d) Summary of peak shift $\Delta\lambda$ and SERS intensity I_{1500} for two different strategies. Statistics were obtained from 3 measurements (n = 3) of transmission and 15 measurements (n = 15) of SERS.

concentration of SM is 1 order of magnitude higher than that of T, so the SERS results still show a good specificity of T compared to SM. Figure 8d summarizes the dip shift $\Delta\lambda$ due to

index change and SERS intensity change ΔI_{1500} after targeting T, SM, and UM. It shows that the relative signal ratio $\Delta \lambda^{\rm SM}/\Delta \lambda^{\rm T}(\sim 0)$ and $\Delta \lambda^{\rm UM}/\Delta \lambda^{\rm T}(\sim 0.1)$ due to index sensing is much

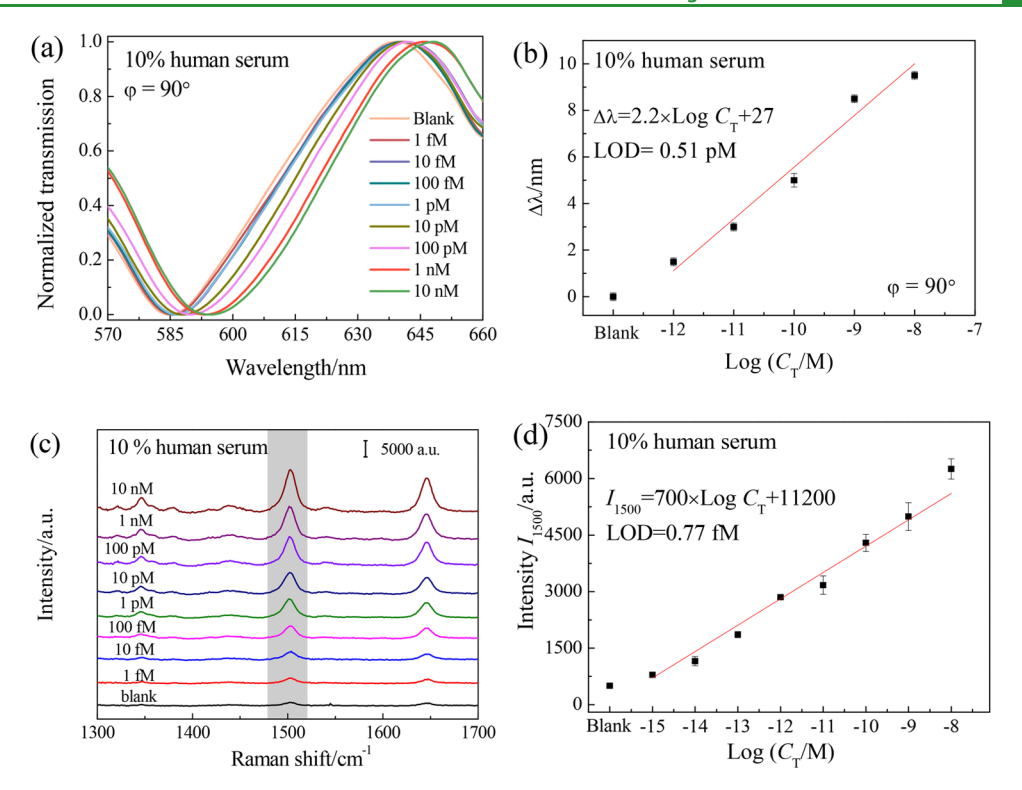


Figure 10. SERS/SPR dual-mode sensor performance by detecting DNA T-spiked 10% human serum samples. (a) Concentration-dependent normalized transmission spectra ($\varphi = 90^{\circ}$). (b) Plot of $\Delta\lambda$ versus $\log(C_{\rm T})$. Statistics were obtained from three measurements (n = 3). (c) Corresponding concentration-dependent SERS spectra and (d) the plot of I_{1500} versus $\log(C_{\rm T})$. Statistics were obtained from 15 measurements (n = 15).

smaller than the respective $I_{1500}^{\rm SM}/I_{1500}^{\rm T}$ (\sim 0.11) and $I_{1500}^{\rm IM}/I_{1500}^{\rm T}$ (\sim 0.63). Therefore, the SPR mode has a better specificity than that of the SERS mode. The reason why the SERS mode has a worse specificity compare to that of SPR is that there are two parts of the signal that contribute to the real SERS signal at high molecular concentration: the SERS signals from molecules adsorbed in the hot spots and the Raman signals from all the molecules residing in the laser excitation area during the measurement. It is expected that more SM and UM molecules will adsorb on the Ag NR-NH array due to its high surface area; thus, more normal Raman signals would be produced. Meanwhile, the SPR mode is insensitive to the molecules not adsorbed in the SPR hot spot. Therefore, the SPR mode has a higher specificity.

3.3.3. Sensitivity Enhancement of the DNA Supersandwich Strategy. The sensitivity enhancement of the proposed DNA supersandwich assay using the DNA concatamers compared to the normal sandwich strategy using ssDNA S1 was investigated. Both strategies use the TDP-modified Ag NR-NH array immersed in 100 pM DNA T followed by further hybridization with two different sandwich assays, the DNA concatamers and the ssDNA S1. The corresponding transmission spectra (φ = 90°) are shown in Figure 9a,b. The $\Delta \lambda = 0.50 \pm 0.08$ nm for using the DNA concatamer strategy (Figure 9a) is almost 10 times that $(\Delta \lambda = 5.0 \pm 0.2 \text{ nm})$ for the ssDNA S1 strategy (Figure 9b), indicating that the sensing signal is amplified 10 times (Figure 9d) by using the DNA concatamers compared to the normal ssDNA S1 sandwich sensing strategy. Such an enhanced sensitivity is mainly due to the bigger RI change induced by immobilizing the larger double-stranded DNA concatamers with respect to the shorter ssDNA S1. Similarly, the corresponding SERS peak intensities are also enhanced, as shown in Figure 9c, due to the fact that more DNAs are immobilized on the surface for the DNA concatamer strategy. As summarized in Figure 9d, the $I_{1500} = 5300 \pm 276$ a.u. for the DNA concatamer strategy is about 4 times that ($I_{1500} = 1300 \pm 134$ a.u.) for the ssDNA S1 strategy.

3.4. Practicability of the SERS/SPR Dual-Mode Sensing. The practicability of the SERS/SPR dual-mode sensor was verified by detecting the DNA T spiked in 10% human serum followed by the DNA supersandwich strategy. First, the calibration curves of detection signals versus C_T (from 1 fM to 10 nM) in the human serum were established. Figure 10a,b shows the concentration-dependent normalized transmission spectra and a semi-log plot of the shift $\Delta \lambda$ of V_2 versus C_T from 1 pM to 10 nM for the SPR mode. The linear fit in Figure 10b gives $\Delta \lambda = 2.2 \times \log C_T + 27 \ (R^2 = 0.969)$, with an LOD of 0.51 pM, very similar to the results obtained in Figure 6f. Figure 10c shows the concentration-dependent SERS spectra, and Figure 10d plots the SERS peak intensity I_{1500} versus $\log(C_{\rm T})$ from 1 fM to 10 nM. Also, a linear relationship, $I_{1500} = 700 \times \log C_T + 11,200$ $(R^2 = 0.978)$ with an LOD of 0.77 fM, is obtained. The results are similar to those obtained from Figure 7b but with lower sensitivity and larger LOD. This is understandable since there could be strong background interference from the human serum. According to the obtained calibration curves, the recovery of the sensor was investigated by detecting $C_T = 7$ pM, 30 pM, and 3 nM spiked 10% human serum samples, and the results are shown in Figure S6 and Table 1. The recovery of the SPR mode-based sensor is 98.37-113.5% and that of the SERS mode assay is 94.43-107.0%, which indicates that the dual-mode sensor has a very good reliability. The recovery for the SPR mode is slightly higher than that of the SERS mode, further indicating the advantage of the complement performance for the two sensors.

Table 1. Recovery of the SERS/SPR Dual-Mode Sensing

sample number	added	found	recovery	RSD	sensing mode
1	7 pM	6.88 pM	98.37%	5.26%	SPR
		6.63 pM	94.71%	7.50%	SERS
2	30 pM	32.62 pM	108.7%	5.80%	SPR
		28.33 pM	94.43%	3.59%	SERS
3	3 nM	3.40 nM	113.5%	1.92%	SPR
		3.21 nM	107.0%	6.85%	SERS

Clearly, the dual-mode sensor can provide redundant sensing with complimentary sensing performances, which effectively improves the sensitivity, specificity, and reliability of the sensor. Such a strategy could significantly reduce the false alarm rate for practical applications.

4. CONCLUSIONS

A novel SERS/SPR dual-mode biosensor was prepared on the Ag NR-NH array for highly sensitive and reliable DNA detection. The specificity of the sensor was guaranteed by modifying the surface of the nanostructures with tetrahedral DNA probes, and the sensing signal was further amplified using a DNA supersandwich strategy. The proposed DNA supersandwich sensing strategy can provide about 10 and 4 times signal enhancements of SPR and SERS sensing, respectively. The proposed dual-mode sensor has a complementary sensor performance: the SPR mode sensor provides high specificity and recovery, while the SERS ensures high sensitivity. In particular, for detecting DNA T from spiked human serum samples, the LODs for SPR and SERS modes are 0.51 pM and 0.77 fM, while the corresponding recoveries are 98.37-113.5 and 94.43-107.0%, respectively. Clearly, the sensor structures are not optimized. There are many strategies that could be used to further improve the sensitivity and reliability of the dual-mode sensors, for example, improving the SPR sensitivity by elevating the nanohole structure ²² or further optimizing the sensitivity for the SERS mode. The redundant detection signals from the two modes can provide more reliable data to prevent false-positive or false-negative detections, thus further improving the overall performance of the sensor. In addition, benefiting from the programmability of the tetrahedral DNA probes, the SERS/SPR dual-mode biosensor can be utilized to detect other crucial DNA/RNA (e.g., disease-related nucleic acids) with different base numbers by adjusting the bases of the ssDNAs, which were used to assemble the tetrahedral DNA probe, according to the base species and numbers of target nucleic acids. It is expected that such a dual-mode sensor has a great potential for many applications, such as medical diagnostics, food safety, national security, etc.

ASSOCIATED CONTENT

Supporting Information

The Supporting Information is available free of charge at https://pubs.acs.org/doi/10.1021/acsami.0c08453.

Single-stranded DNA (ssDNA) sequences (Tables S1), XRD pattern (Figure S1), polarization-dependent transmission spectra (Figure S2), EF calculation (Figure S3), step-by-step monitoring of the surface modification of Ag NR-NH by SPR (Figure S4), uniformity of the SERS sensing (Figure S5), and recovery of SERS/SPR dualmode sensing (Figure S6) (PDF)

AUTHOR INFORMATION

Corresponding Author

Lianhui Wang - Key Laboratory for Organic Electronics and Information Displays & Jiangsu Key Laboratory for Biosensors, Institute of Advanced Materials (IAM), Jiangsu National Synergetic Innovation Center for Advanced Materials (SICAM), Nanjing University of Posts & Telecommunications, Nanjing 210023, China; orcid.org/0000-0001-9030-9172; Email: iamlhwang@njupt.edu.cn

Authors

Chunyuan Song – Key Laboratory for Organic Electronics and Information Displays & Jiangsu Key Laboratory for Biosensors, Institute of Advanced Materials (IAM), Jiangsu National Synergetic Innovation Center for Advanced Materials (SICAM), Nanjing University of Posts & Telecommunications, Nanjing 210023, China; orcid.org/0000-0001-9111-1029

Xinyu Jiang - Key Laboratory for Organic Electronics and Information Displays & Jiangsu Key Laboratory for Biosensors, Institute of Advanced Materials (IAM), Jiangsu National Synergetic Innovation Center for Advanced Materials (SICAM), Nanjing University of Posts & Telecommunications, Nanjing 210023, China

Yanjun Yang - Key Laboratory for Organic Electronics and Information Displays & Jiangsu Key Laboratory for Biosensors, Institute of Advanced Materials (IAM), Jiangsu National Synergetic Innovation Center for Advanced Materials (SICAM), Nanjing University of Posts & Telecommunications, Nanjing 210023, China; Department of Physics and Astronomy, University of Georgia, Athens, Georgia 30602, United States

Jingjing Zhang - Key Laboratory for Organic Electronics and Information Displays & Jiangsu Key Laboratory for Biosensors, Institute of Advanced Materials (IAM), Jiangsu National Synergetic Innovation Center for Advanced Materials (SICAM), Nanjing University of Posts & Telecommunications, Nanjing 210023, China

Steven Larson — Department of Physics and Astronomy, University of Georgia, Athens, Georgia 30602, United States **Yiping Zhao** – Department of Physics and Astronomy, University of Georgia, Athens, Georgia 30602, United States; o orcid.org/ 0000-0002-3710-4159

Complete contact information is available at: https://pubs.acs.org/10.1021/acsami.0c08453

Author Contributions

The manuscript was written through contributions of all authors. All authors have given approval to the final version of the manuscript.

Notes

The authors declare no competing financial interest.

ACKNOWLEDGMENTS

C.S., L.W., and J.Z. were supported by the National Key Research and Development Program of China (2017YFA0205300), the National Natural Science Foundation of China (61871236 and 61971207), the Natural Science Foundation of Jiangsu Province of China (BK20181395), and the Key Research and Development Program of Jiangsu (BE2018732). X.J. was supported by the Postgraduate Research and Practice Innovation Program of Jiangsu Province (KYCX18_0858). Y.Y., S.L., and Y.Z. were supported by the

National Natural Science Foundation (ECCS-1609815 and ECCS-1808271).

REFERENCES

- (1) Pan, X.; Li, L.; Lin, H.; Tan, J.; Wang, H.; Liao, M.; Chen, C.; Shan, B.; Chen, Y.; Li, M. A Graphene Oxide-Gold Nanostar Hybrid Based-Paper Biosensor for Label-Free SERS Detection of Serum Bilirubin for Diagnosis of Jaundice. *Biosens. Bioelectron.* **2019**, *145*, 111713.
- (2) Pang, Y.; Wang, C.; Lu, L.; Wang, C.; Sun, Z.; Xiao, R. Dual-SERS Biosensor for One-Step Detection of MicroRNAs in Exosome and Residual Plasma of Blood Samples for Diagnosing Pancreatic Cancer. *Biosens. Bioelectron.* **2019**, *130*, 204–213.
- (3) Song, N.; Zhao, L.; Xu, X.; Zhu, M.; Liu, C.; Sun, N.; Yang, J.; Shi, X.; Zhao, J. LyP-1-Modified Multifunctional Dendrimers for Targeted Antitumor and Antimetastasis Therapy. *ACS Appl. Mater. Interfaces* **2020**, *12*, 12395–12406.
- (4) Shao, H.; Lin, H.; Guo, Z.; Lu, J.; Jia, Y.; Ye, M.; Su, F.; Niu, L.; Kang, W.; Wang, S.; Hu, Y.; Huang, Y. J. A Multiple Signal Amplification Sandwich-Type SERS Biosensor for Femtomolar Detection of MiRNA. *Biosens. Bioelectron.* **2019**, *143*, 111616.
- (5) Kneipp, K.; Wang, Y.; Kneipp, H.; Perelman, L. T.; Itzkan, I.; Dasari, R.; Feld, M. S. Single Molecule Detection Using Surface-Enhanced Raman Scattering (SERS). *Phys. Rev. Lett.* **1997**, 78, 1667–1670.
- (6) Nie, S.; Emory, S. R. Probing Single Molecules and Single Nanoparticles by Surface-Enhanced Raman Scattering. *Science* **1997**, 275, 1102.
- (7) Jiang, J.; Zou, S.; Ma, L.; Wang, S.; Liao, J.; Zhang, Z. Surface-Enhanced Raman Scattering Detection of Pesticide Residues Using Transparent Adhesive Tapes and Coated Silver Nanorods. ACS Appl. Mater. Interfaces 2018, 10, 9129–9135.
- (8) Wang, J.; Li, J.; Zeng, C.; Qu, Q.; Wang, M.; Qi, W.; Su, R.; He, Z. Sandwich-Like Sensor for the Highly Specific and Reproducible Detection of Rhodamine 6G on a Surface-Enhanced Raman Scattering Platform. ACS Appl. Mater. Interfaces 2020, 12, 4699—4706.
- (9) Men, D.; Liu, G.; Xing, C.; Zhang, H.; Xiang, J.; Sun, Y.; Hang, L. Dynamically Tunable Plasmonic Band for Reversible Colorimetric Sensors and Surface-Enhanced Raman Scattering Effect with Good Sensitivity and Stability. ACS Appl. Mater. Interfaces 2020, 12, 7494—7503.
- (10) Chen, J.; Wu, Y.; Fu, C.; Cao, H.; Tan, X.; Shi, W.; Wu, Z. Ratiometric SERS Biosensor for Sensitive and Reproducible Detection of MicroRNA Based on Mismatched Catalytic Hairpin Assembly. *Biosens. Bioelectron.* **2019**, *143*, 111619.
- (11) Akkilic, N.; Geschwindner, S.; Höök, F. Single-Molecule Biosensors: Recent Advances and Applications. *Biosens. Bioelectron.* **2020**, *151*, 111944.
- (12) Song, C.; Chen, J.; Abell, J.; Cui, Y.; Zhao, Y. Ag-SiO₂ Core-Shell Nanorod Arrays: Morphological, Optical, SERS, and Wetting Properties. *Langmuir* **2012**, *28*, 1488–1495.
- (13) Nath, S. Exploiting Redundancy for Robust Sensing. Ph.D. Dissertation, Carnegie Mellon University, Pittsburgh, PA, US, 2005.
- (14) Dyankov, G.; Zekriti, M.; Bousmina, M. Dual-Mode Surface-Plasmon Sensor Based on Bimetallic Film. *Appl. Opt.* **2012**, *51*, 2451–2456
- (15) Guo, J.; Keathley, P. D.; Hastings, J. T. Dual-Mode Surface-Plasmon-Resonance Sensors Using Angular Interrogation. *Opt. Lett.* **2008**, 33, 512–514.
- (16) Potara, M.; Gabudean, A. M.; Astilean, S. Solution-Phase, Dual LSPR-SERS Plasmonic Sensors of High Sensitivity and Stability Based on Chitosan-Coated Anisotropic Silver Nanoparticles. *J. Mater. Chem.* **2011**, *21*, 3625–3633.
- (17) Lee, K.-L.; Hung, C.-Y.; Pan, M.-Y.; Wu, T.-Y.; Yang, S.-Y.; Wei, P.-K. Dual Sensing Arrays for Surface Plasmon Resonance (SPR) and Surface-Enhanced Raman Scattering (SERS) Based on Nanowire/Nanorod Hybrid Nanostructures. *Adv. Mater. Interfaces* **2018**, *5*, 1801064.

- (18) Gordon, R.; Sinton, D.; Kavanagh, K. L.; Brolo, A. G. A New Generation of Sensors Based on Extraordinary Optical Transmission. *Acc. Chem. Res.* **2008**, *41*, 1049–1057.
- (19) Masson, J.-F.; Murray-Méthot, M.-P.; Live, L. S. Nanohole Arrays in Chemical Analysis: Manufacturing Methods and Applications. *Analyst* **2010**, *135*, 1483–1489.
- (20) Prasad, A.; Choi, J.; Jia, Z.; Park, S.; Gartia, M. R. Nanohole Array Plasmonic Biosensors: Emerging Point-of-Care Applications. *Biosens. Bioelectron.* **2019**, 130, 185–203.
- (21) Brolo, A. G.; Gordon, R.; Leathem, B.; Kavanagh, K. L. Surface Plasmon Sensor Based on the Enhanced Light Transmission Through Arrays of Nanoholes in Gold Films. *Langmuir* **2004**, *20*, 4813–4815.
- (22) Ai, B.; Basnet, P.; Larson, S.; Ingram, W.; Zhao, Y. Plasmonic Sensor with High Figure of Merit Based on Differential Polarization Spectra of Elliptical Nanohole Array. *Nanoscale* **2017**, *9*, 14710–14721.
- (23) Carney, D. J.; Svavarsson, H. G.; Hemmati, H.; Fannin, A.; Yoon, J. W.; Magnusson, R. Refractometric Sensing with Periodic Nano-Indented Arrays: Effect of Structural Dimensions. *Sensors* **2019**, *19*, 897.
- (24) Correia-Ledo, D.; Gibson, K. F.; Dhawan, A.; Couture, M.; Vo-Dinh, T.; Graham, D.; Masson, J.-F. Assessing the Location of Surface Plasmons over Nanotriangle and Nanohole Arrays of Different Size and Periodicity. *Phys. Chem. C* **2012**, *116*, 6884–6892.
- (25) Choi, W.; Jo, Y.; Ahn, J.; Seo, E.; Park, Q.-H.; Jhon, Y. M.; Choi, W. Control of Randomly Scattered Surface Plasmon Polaritons for Multiple-Input and Multiple-Output Plasmonic Switching Devices. *Nat. Commun.* **2017**, *8*, 14636.
- (26) Larson, S.; Luong, H.; Song, C.; Zhao, Y. Dipole Radiation-Induced Extraordinary Optical Transmission for Silver Nanorod-Covered Silver Nanohole Arrays. *J. Phys. Chem. C* **2019**, 123, 5634–5641.
- (27) Liu, Y.-J.; Chu, H. Y.; Zhao, Y.-P. Silver Nanorod Array Substrates Fabricated by Oblique Angle Deposition: Morphological, Optical, and SERS Characterizations. *J. Phys. Chem. C* **2010**, *114*, 8176–8183.
- (28) Driskell, J. D.; Seto, A. G.; Jones, L. P.; Jokela, S.; Dluhy, R. A.; Zhao, Y.-P.; Tripp, R. A. Rapid MicroRNA (miRNA) Detection and Classification via Surface-Enhanced Raman Spectroscopy (SERS). *Biosens. Bioelectron.* **2008**, *24*, 917–922.
- (29) Driskell, J. D.; Primera-Pedrozo, O. M.; Dluhy, R. A.; Zhao, Y.; Tripp, R. A. Quantitative Surface-Enhanced Raman Spectroscopy Based Analysis of MicroRNA Mixtures. *Appl. Spectrosc.* **2009**, *63*, 1107–1114.
- (30) Abell, J. L.; Garren, J. M.; Driskell, J. D.; Tripp, R. A.; Zhao, Y. Label-Free Detection of Micro-RNA Hybridization Using Surface-Enhanced Raman Spectroscopy and Least-Squares Analysis. *J. Am. Chem. Soc.* **2012**, *134*, 12889–12892.
- (31) Song, C. Y.; Yang, Y. J.; Yang, B. Y.; Sun, Y. Z.; Zhao, Y. P.; Wang, L. H. An Ultrasensitive SERS Sensor for Simultaneous Detection of Multiple Cancer-Related MiRNAs. *Nanoscale* **2016**, *8*, 17365–17373.
- (32) Zhang, J.; Yang, Y.; Jiang, X.; Dong, C.; Song, C.; Han, C.; Wang, L. Ultrasensitive SERS Detection of Nucleic Acids *via* Simultaneous Amplification of Target-Triggered Enzyme-Free Recycling and Multiple-Reporter. *Biosens. Bioelectron.* **2019**, *141*, 111402.
- (33) Pei, H.; Lu, N.; Wen, Y.; Song, S.; Liu, Y.; Yan, H.; Fan, C. A DNA Nanostructure-Based Biomolecular Probe Carrier Platform for Electrochemical Biosensing. *Adv. Mater.* **2010**, *22*, 4754–4758.
- (34) Lin, M.; Wang, J.; Zhou, G.; Wang, J.; Wu, N.; Lu, J. X.; Gao, J.; Chen, X.; Shi, J.; Zuo, X.; Fan, C. Programmable Engineering of a Biosensing Interface with Tetrahedral DNA Nanostructures for Ultrasensitive DNA Detection. *Angew. Chem. Int. Ed.* **2015**, *54*, 2151–2155.
- (35) Yang, Y.; Jiang, X.; Chao, J.; Song, C.; Liu, B.; Zhu, D.; Sun, Y.; Yang, B.; Zhang, Q.; Chen, Y.; Wang, L. Synthesis of Magnetic Core-Branched Au Shell Nanostructures and Their Application in Cancer-Related MiRNA Detection via SERS. Sci. China Mater. 2017, 60, 1129—1144.
- (36) Diao, W.; Tang, M.; Ding, S. J.; Li, X.; Cheng, W.; Mo, F.; Yan, X.; Ma, H.; Yan, Y. Highly Sensitive Surface Plasmon Resonance Biosensor

- for the Detection of HIV-Related DNA Based on Dynamic and Structural DNA Nanodevices. *Biosens. Bioelectron.* **2018**, *100*, 228–234. (37) Zhang, Y.; Shuai, Z.; Zhou, H.; Luo, Z.; Liu, B.; Zhang, Y. N.; Zhang, L.; Chen, S.; Chao, J.; Weng, L. M.; Fan, Q.; Fan, C.; Huang, W.; Wang, L. Single-Molecule Analysis of MicroRNA and Logic Operations Using a Smart Plasmonic Nanobiosensor. *J. Am. Chem. Soc.* **2018**, *140*, 3988–3993.
- (38) He, Y.; Larsen, G.; Ingram, W.; Zhao, Y. Tunable Three-Dimensional Helically Stacked Plasmonic Layers on Nanosphere Monolayers. *Nano Lett.* **2014**, *14*, 1976–1981.
- (39) Song, C.; Abell, J.; He, Y.; Murph, S. H.; Cui, Y.; Zhao, Y. Gold-Modified Silver Nanorod Arrays: Growth Dynamics and Improved SERS Properties. *J. Mater. Chem.* **2012**, *22*, 1150–1159.
- (40) Driskell, J. D.; Shanmukh, S.; Liu, Y.; Chaney, S. B.; Tang, X.-J.; Zhao, Y.-P.; Dluhy, R. A. The Use of Aligned Silver Nanorod Arrays Prepared by Oblique Angle Deposition as Surface Enhanced Raman Scattering Substrates. *J. Phys. Chem. C* **2008**, *112*, 895–901.
- (41) Zhao, Y.-P.; Chaney, S. B.; Zhang, Z.-Y. Absorbance Spectra of Aligned Ag Nanorod Arrays Prepared by Oblique Angle Deposition. *J. Appl. Phys.* **2006**, *100*, No. 063527.
- (42) Song, C.; Yang, B.; Zhu, Y.; Yang, Y.; Wang, L. Ultrasensitive Sliver Nanorods Array SERS Sensor for Mercury Ions. *Biosens. Bioelectron.* **2017**, 87, 59–65.